https://doi.org/10.5194/bg-2019-426
Preprint. Discussion started: 14 November 2019

Biogeosciences Discussions

Vivianite formation in ferruginous sediments from Lake Towuti, Indonesia.

Aurèle Vuillemin[1,2], André Friese[1], Richard Wirth[1], Jan A. Schuessler[1], Anja M. Schleicher[1], Helga Kemnitz[1], Andreas Lücke[3], Kohen W. Bauer[4,5], Sulung Nomosatryo[1,6], Friedhelm von Blanckenburg[1], Rachel Simister[4], Luis G. Ordoñez[7], Daniel Ariztegui[7], Cynthia Henny[6], James M. Russell[8], Satria Bijaksana[9], Hendrik Vogel[10], Sean A. Crowe[4,5,11], Jens Kallmeyer[1] and the Towuti Drilling Project Science Team*.

[1]GFZ German Research Centre for Geosciences, Helmholtz Centre Potsdam, Potsdam, 14473, Germany
[2]Present address: Department of Earth and Environmental Science, Paleontology and Geobiology, Ludwig-Maximilians-Universität München, Munich, 80333, Germany
[3]Research Center Jülich, Institute of Bio- and Geosciences 3: Agrosphere, Jülich, 52428, Germany
[4]Department of Earth, Ocean, and Atmospheric Sciences, University of British Columbia, Vancouver, BC, V6T 1Z4, Canada
[5]Present address: Department of Earth Sciences, University of Hong Kong, Hong Kong, China
[6]Research Center for Limnology, Indonesian Institute of Sciences (LIPI), Cibinong-Bogor, Indonesia
[7]Department of Earth Sciences, University of Geneva, Geneva, 1205, Switzerland
[8]Department of Earth, Environmental, and Planetary Sciences, Brown University, 13 Providence, RI, 02912, USA
[9]Faculty of Mining and Petroleum Engineering, Institut Teknologi Bandung, 15 Bandung, 50132, Indonesia
[10]Institute of Geological Sciences and Oeschger Centre for Climate Change Research, University of Bern, CH-3012, Bern, Switzerland
[11]Department of Microbiology and Immunology, University of British Columbia, Vancouver, BC, V6T 1Z3, Canada
*A full list of authors appears at the end of the paper

Correspondence to: Aurèle Vuillemin (a.vuillemin@lrz.uni-muenchen.de)

Abstract. Ferruginous lacustrine systems, such as Lake Towuti, Indonesia, can experience restricted primary production due to phosphorus trapping by hydrous ferric iron (oxyhydr)oxides that reduce P concentrations in the water column. The oceans were also ferruginous during the Archean, so understanding the dynamics of phosphorus in modern-day ferruginous analogues may shed light on the marine biogeochemical cycling that dominated much of Earth's history. Here we report the presence of large crystals (>5 mm) and nodules (>5 cm) of vivianite – a ferrous iron phosphate – in sediment cores from Lake Towuti, and address the processes of phosphorus retention and iron mineral transformations during diagenesis in ferruginous sediments.

Core scans together with analyses of bulk sediment and pore water geochemistry document a 30 m long interval consisting of beds of sideritic and non-sideritic clays and diatomaceous oozes containing diagenetic vivianites. High-resolution imaging of vivianite revealed continuous growth of crystals from tabular to rosette habits that eventually form large (up to 7 cm) vivianite nodules in the sediment. Mineral inclusions like millerite and siderite reflect antecedent diagenetic mineral formation that is related to microbial reduction of iron and sulfate. This implies the formation and growth of vivianite crystals under reducing conditions during diagenesis. Negative δ^{56}Fe values of vivianite indicated reductive dissolution of ferric oxides as the source of Fe in the vivianites with incorporation of microbially fractionated light Fe^{2+} into the crystals.

https://doi.org/10.5194/bg-2019-426
Preprint. Discussion started: 14 November 2019

Biogeosciences Discussions Open Access EGU

The size and growth history of the nodules indicate that, after formation, continued growth of vivianite may constitute a significant sink for P in these sediments.

1 Introduction

In the lacustrine realm, phosphorus (P) is often the limiting nutrient for primary production (Compton et al., 2000). Its supply to primary producers in the euphotic zone depends on external fluxes (Manning et al., 1999; Zegeye et al., 2012) and internal recycling as a result of organic matter (OM) mineralization in both the water column and underlying sediments (Katsev et al., 2006; Hupfer and Lewandowski, 2008). Removal of phosphate through burial in sediments depends partly on sorption to iron oxides (Wilson et al., 2010), and because iron oxides tend to dissolve under anoxia, phosphate burial is sensitive to the oxygenation state of the water column and water-sediment interface (Sapota et al., 2006; Rothe et al., 2015). In environments with high sulfate (SO_4^{2-}) concentrations microbial SO_4^{2-} reduction usually leads to the formation of iron sulfides that decrease Fe-recycling and the formation of Fe (oxyhydr)oxides in the upper oxygenated sediments, and this in turn decreases the extent to which P is retained in the sediment (Roden and Edmonds, 1997). Formation of iron phosphate minerals such as vivianite (i.e. $Fe_3(PO_4)_2 \cdot 8H_2O$) in response to the accumulation of sedimentary Fe and P (Gächter et al., 1988; Wilson et al., 2010; Rothe et al., 2016) is a less-studied process that, in contrast, can contribute to long-term P retention in the sediment, particularly in ferruginous (anoxic, non-sulfidic) environments (Gächter and Müller, 2003). Although anoxia is commonly thought to promote P release from sediments and its recycling back to the photic zone of the water column, the high ferrous iron concentrations that can develop in ferruginous environments may promote the formation of iron phosphate minerals, thereby restricting P recycling and bioavailability.

Vivianite is a common phosphate mineral in lacustrine systems (Vuillemin et al., 2013; Rothe et al., 2015). It regularly occurs in organic-rich sediments, often in close association with macroscopic organic remains, and when production of sulfide is low (Rothe et al., 2016). Although it is common in eutrophic lakes, presumably due to high P concentrations, its occurrence in ferruginous, oligotrophic lakes, which may be similar to the Archean oceans, is poorly known. In such systems, high Fe concentrations should catalyse vivianite formation, yet low P concentrations may preclude its formation. As reported from laboratory studies, vivianite nucleation is possible under relatively high concentrations of Fe^{2+} and orthophosphate (solubility product: $Ksp = 10^{-36}$) at pH between 6 and 9 (Glasauer et al., 2003; Rothe et al., 2014; Sánchez-Román et al., 2015). It thus forms as a secondary mineral product in response to iron reduction when P concentrations are sufficiently high (Fredrickson et al., 1998; Zachara et al., 1998; O'Loughlin et al., 2013). Despite these requirements, vivianite formation is not restricted to any specific trophic state or salinity range and has been shown to form under a broad range of bottom water redox conditions in freshwater and marine environments (Egger et al., 2015; Dijkstra et al., 2016).

In the humid tropics, deep and intense chemical weathering of bedrock often leads to the formation of thick laterite soils residually enriched in iron (oxyhydr)oxides that promote P scavenging (Lemos et al., 2007). Erosion of these soils and subsequent delivery to lakes promotes P deposition and retention in lake sediments (Fagel et al., 2005; Sapota et al., 2006;

https://doi.org/10.5194/bg-2019-426
Preprint. Discussion started: 14 November 2019

Rothe et al., 2014). One of such environment is the ancient Malili Lake System, Sulawesi, Indonesia (Lehmusluoto et al., 1995; Haffner et al., 2001), whose catchment is dominated by ultramafic bedrock overlain by thick lateritic soils (Golightly et al., 2010; Morlock et al., 2019). The Malili Lakes are presently characterized by a dearth of SO_4^{2-} (Crowe et al., 2004; Vuillemin et al., 2016) and low biomass (Bramburger et al., 2008), likely because fluxes of iron (oxyhydr)oxides from surrounding soils scavenge P in the soils, rivers and lake surface waters (Crowe et al., 2008; Katsev et al., 2010; Zegeye et al., 2012). In Lake Towuti, environmental and sedimentary processes, such as weathering intensity (Russell et al., 2014; Morlock et al., 2019), lake mixing and bottom water oxygenation (Costa et al., 2015), and fluctuations in lake level and deltaic sedimentation (Vogel et al., 2015; Hasberg et al., 2019) have changed through time and altered the abundance of reactive ferric iron, and potentially P, in the water column and sediment. However, P dynamics have not been intensively studied in this lake.

On the short term, P retention in lake sediments mainly depends on the oxygenation of the water column (Reed et al., 2016), with depletion of the reducible iron pool under oxygen-poor conditions resulting in the release of accumulated P from the sediment (Katsev et al., 2006). For instance in 600 m deep permanently stratified Lake Matano (Crowe et al., 2008), microbial reduction of iron, which takes place below the modern-day oxycline, leads to partial release of adsorbed P into the bottom water and its accumulation over time (Crowe et al., 2008). Like Lake Matano, Lake Towuti, the largest of the Malili Lakes, presently displays an extreme scarcity of SO_4^{2-} (<20 μM), nitrate/nitrite (<5 μM), phosphate (PO_4^{3-} <5 μM) and oxygen depletion below ~130 m water depth (Vuillemin et al., 2016). Evidence for a complete overturn of the water column is absent in recent years, but sediment data indicate that periods of complete overturn and bottom water oxygenation may have occurred in the geological past (Costa et al., 2015). In an oxygenated water column, hydrous ferric oxides could reach the water-sediment interface and prevent P and Fe release from the sediment (Shaffer, 1986; Katsev et al., 2006). In contrast, anoxia should favour the release of P and Fe from surface sediments and pore waters back to the anoxic bottom water, which would fundamentally change the lake's biology. Even though the lake is presently stratified, PO_4^{3-} in the modern anoxic lake is extraordinarily low, implying a sink for P that is stable under anoxic conditions, like vivianite. Sediment drill core data, furthermore, indicate that Lake Towuti has undergone large changes in primary productivity through time, suggesting very different P biogeochemical cycling in the past, possibly linked to dynamics in sediment P mineralogy.

The Malili Lakes, including Lake Towuti, thus represent a relevant setting in which to explore the distribution and characteristics of vivianite formed under Fe-rich and fluctuating redox conditions. From May to July 2015, the Towuti Drilling Project (TDP) recovered more than 1000 m of sediment drill core from three sites in Lake Towuti, including a 113-m-long core dedicated to geomicrobiological studies at site TDP-TOW15-1A (Russell et al., 2016; Friese et al., 2017). The discovery of sedimentary beds containing large vivianite crystals in this core prompted the present study investigating the distribution and characteristics of vivianite and the modes of vivianite formation in response to environmental variability.

https://doi.org/10.5194/bg-2019-426
Preprint. Discussion started: 14 November 2019

2 Methods

2.1 Study site and drilling operations

Lake Towuti (2.5°S, 121°E) is a 200 m deep lake that is part of the Malili Lake System (Fig. 1), a chain of five interconnected tectonic lakes seated in ophiolitic rocks covered with thick lateritic soils on Sulawesi Island, Indonesia (Lehmusluoto et al., 1995; Haffner et al., 2001). The Mahalona River, which is Lake Towuti's main inflow to the north, connects to the upstream Lakes Mahalona and Matano, while the Larona River constitutes Lake Towuti's only outflow to the west (Vogel et al., 2015). Lake Towuti's water column is circumneutral (pH = 8.4 to 7.2), weakly thermally stratified (i.e. 31-28°C) and presently oxygen-depleted below ~130 m depth (Nomosatryo et al., 2013). The water chemistry is dominated by Mg^{2+} and HCO_3^- ions (Lehmusluoto et al., 1995; Haffner et al., 2001).

The TDP coring operations were carried out using the International Continental Scientific Drilling Program (ICDP) Deep Lakes Drilling System (Russell et al., 2016). In the field, core catchers from TDP-TOW15-1A (156 m water depth; hereafter TDP-1A) were packed into gas-tight aluminum foil bags flushed with nitrogen gas and heat-sealed to keep them under anoxic conditions until mineral extraction. Pore water was extracted on site from 5-cm-long whole round cores (6.6 cm diameter) that were cut from the core sections, immediately capped and transferred to an anaerobic chamber flushed with nitrogen to avoid oxidation during sample handling (Friese et al., 2017). In February 2016, the unsampled remainders of the cores from TDP-1A were split and scanned at the Limnological Research Center, Lacustrine Core Facility (LacCore), University of Minnesota, described macroscopically and microscopically to determine their stratigraphy and composition (Russell et al., 2016) and then subsampled. Except as otherwise noted, all our samples and measurements come primarily from hole TDP-1A.

2.2 Total organic carbon

Sediment from core catchers from TDP-1A was used to quantify total organic carbon (TOC). Sediment samples were freeze-dried prior to analysis. Carbonate minerals were removed by treating the samples with 20 mL of 5 % HCl at 50º C for 24 hours (Golubev et al., 2009). Following treatment, samples were repeatedly rinsed with deionized water to reach neutral pH, centrifuged to discard water and freeze-dried. We tested this treatment using 200 mg of technical grade siderite ($FeCO_3$) to evaluate dissolution. Results showed that 85 % of the siderite is efficiently dissolved within the first 2 hours of treatment and 95 to 100 % after 24 hours (Supplementary Fig. S1). About 8 to 10 mg of homogenized decarbonated samples were measured using an elemental analyzer (EuroVector, EuroEA). Combustion was done in an excess of oxygen at 1040 °C. TOC concentrations were calculated from the yield of CO_2 after sample combustion in the elemental analyzer. Analytical precision of the method is ±3 % (1σ) of the yield of CO_2. TOC was recalculated to the content of the whole sample and results are presented in dry mass weight % (wt %).

https://doi.org/10.5194/bg-2019-426
Preprint. Discussion started: 14 November 2019

2.3 Total iron

For reactive Fe sequential extraction, we processed 200 mg of sediment according to Poulton and Canfield (2005). Total Fe was obtained by summing up the highly reactive Fe pools (i.e. sodium acetate, 0.5 N HCl, dithionite, oxalate extractable Fe) and the non-reactive Fe contained in silicate minerals. Our protocol could dissolve >92% of the Fe from the PACS-2 international reference standard, ensuring high Fe yield from the samples. All Fe concentration measurements were performed using a Varian AA875 Flame Atomic Absorption Spectrophotometer (Varian, Palo Alto, USA). Precision on triplicate measurements was 1.2 % and our limit of detection was 1500 µg g^{-1} (0.15 wt % or ~10 µmol cm^{-3}).

2.4 Pore water geochemistry

Within the upper ten meters, pore water was extracted using Rhizon Pore Water Samplers (Rhizosphere research products, Dolderstraat, Netherlands), directly inserted into the soft sediment. Below 10 m depth, we removed the more compact sediment samples from their liner and scraped off all potentially contaminated rims with a sterile scalpel. The remaining sediment was transferred into an IODP-style titanium pore water extraction cylinder (Mannheim et al., 1966) and placed on a 2-column bench top laboratory hydraulic press (Carver Inc., Wabash, USA). Pore water from both shallow and deep sediments was filtered through a sterile 0.2 µm syringe filter and collected in a glass syringe pre-flushed with nitrogen. For anion analysis, 1 mL of pore water was transferred to a screw neck glass vial (VWR International, USA) and stored at 4°C until analysis.

Dissolved iron concentrations were measured in the field via spectrophotometry (Viollier et al., 2000). Directly after pore water retrieval, we aliquoted 1 mL of pore water sample to 1.6 mL Rotilabo single-use cells (Carl Roth, Karlsruhe, Germany) and stabilized dissolved Fe^{2+} by adding 100 µL of Ferrozine Iron Reagent (Sigma-Aldrich Chemie Munich, Germany). Absorbance of the coloured solution was measured at 562 nm with a DR 3900 spectrophotometer (Hach, Düsseldorf, Germany). Detection limit of the method is 0.25 µM. Concentrations of PO_4^{3-} in pore water were measured by suppressed ion chromatography using a SeQuant SAMS anion IC suppressor (EMD Millipore, Billerica, Massachusetts), a S5200 sample injector, a 3.0 × 250 mm LCA 14 column and a S3115 conductivity detector (all Sykam). The eluent was 5 mM Na_2CO_3 with 20 mg L^{-1} 4–hydroxibenzonitrile and 0.2 % methanol. Flow rate was set to 1 mL min^{-1} and column oven temperature to 50 °C. A multi-element anion standard (Sykam) containing PO_4^{3-} (210.6 µM) was diluted 10 times and measured every 10 samples together with a blank sample. Respective minimum detection (signal/noise=3) and quantification limits (S/N=10) for PO_4^{3-} are 4.3 µM and 14.3 µM. The reproducibility was always better than 3 %.

The pH was measured with a portable pH meter (Thermo Scientific Orion, Star A321) calibrated at pH 4, 7 and 10, respectively. We homogenized 2 mL of sediment in 2 mL of deionized water and measured the supernatant after 2 min. Alkalinity was measured via colorimetric titration on a sample of hydraulically squeezed pore water. Dissolved inorganic carbon (DIC) concentrations were calculated by solving the carbonate system using the pH and alkalinity profiles and borehole temperatures.

https://doi.org/10.5194/bg-2019-426
Preprint. Discussion started: 14 November 2019

2.5 Vivianite identification and crystal separation

The drill cores from TDP-1A remaining after field sampling of whole core rounds were split at LacCore, University of Minnesota, USA. Split core halves were imaged at a resolution of 10 pixels/mm (~254 dpi) using a Geotek Geoscan-III with line-scan CCD cameras with fluorescent lights and polarizing filters to reveal core stratigraphy (Russell et al., 2016). The present study is based on macroscopically visible vivianite crystals hand-picked from split TDP-1A cores from 5 distinct horizons located between 20 and 50 m sediment depth. Below and above this interval, vivianites are rarely present in the sediment, which was confirmed by smear slide analysis (Russell et al., 2016) and X-ray diffraction (Supplementary Fig. S2). Additional mineral separates of vivianite were obtained from core catchers. We mixed 50 mL of sediment with deionized water in a beaker and sonicated the slurry to homogenize and break up clay aggregates. The slurry was then separated with an initial settling time of ~2 min and removal of the supernatant. We separated the magnetic from the non-magnetic fraction in the settled dense fraction by placing a neodymium magnet below the beaker and rinsing out the non-magnetic mineral fraction with deionized water, followed by drying with acetone. Minerals observed under a stereo microscope (Nikon SMZ800) included siderite, vivianite, millerite (i.e. NiS) and detrital pyroxene (i.e. $Ca(Mg, Fe)Si_2O_6$). Pyrite (i.e. FeS_2) was not observed.

2.8 X-ray powder diffraction

X-ray diffraction (XRD) patterns were obtained for one concentrated extract of powdered vivianite as well as for 6 samples of freeze-dried bulk sediment from different depths (i.e. 6.3, 12.4, 23.4, 52.7, 66.5, and 82.6 m), using a PANalytical Empyrean X-ray diffractometer (Eindhoven, The Netherlands), operating with a theta-theta goniometer at 40 kV and 40 mA and a PIXcel 3D detector. CuKα radiation was used with a step size from 4.6 to 85° 2Θ and a count time of 1 min per step. The software packages AXS DIFFRACplus EVA and AXS Topas v. 4.2 (both Bruker) were used to identify minerals and select peak references from the mineralogical database.

2.6 Field emission scanning electron microscopy

Isolated crystals of vivianite were mounted on 12.7 mm-diameter aluminum stubs with double-sided conductive carbon tape. An entire vivianite crystal was also embedded in epoxy and the stub cut in axial section. An ultra-thin coating of carbon was deposited on the samples by high-vacuum sputter coating using a Leica MED 020 BAL-TEC metallizer. Imaging was carried out using an Ultra 55 Plus Schottky-type field emission scanning electron microscope. This microscope is equipped with an X-ray energy-dispersive (EDX) system and a Thermo Fisher Scientific silicon-drift detector (SDD UltraDry) for elemental analysis. Operating parameters were set at an acceleration voltage of 20 kV, working distance of 12.5 mm for secondary electron and back-scattering electron images, a 120 mm wide aperture, a silicon-drift detector take-off angle of 35°, and acquisition time of 30 s at a reduced count rate and dead time as needed for point analyses. Calculation of particle chemistry was performed by applying the procedure of the Noran System Seven software based on the standardless matrix correction

https://doi.org/10.5194/bg-2019-426
Preprint. Discussion started: 14 November 2019

methods ZAF (i.e. atomic number, absorption, fluorescence) and φ(ρz). Quantitative analyses of all detectable elements were normalized to 100 % atomic weight displayed as oxides. The detection limit for EDX ranges between 0.1 and 1 wt %.

2.7 Transmission electron microscopy

Preparation of electron-transparent vivianite samples was done with a FEI FIB200TEM focused ion beam (FIB) device. A TEM-ready foil with final dimensions of 15 × 10 × 0.1 µm was cut directly from the carbon-coated polished section using a gallium ion beam under high-vacuum conditions and placed on a carbon film on top of a copper grid. Carbon-coating to prevent charging of the TEM sample was not applied (Wirth, 2009). The FIB-cut TEM foil was surveyed and analyzed using a FEI Tecnai G^2 F20 X-Twin transmission electron microscope. The microscope is equipped with an EDAX ultra-thin window EDX system, a Fishione high-angle annular dark-field (HAADF) detector, and a Gatan imaging filter. Operating conditions were set to an acceleration voltage of 200 kV, using normal imaging mode for bright-field and dark-field imaging and scanning transmission electron microscopy mode for HAADF imaging and analytical electron microscopy. All HAADF images were acquired with a camera length of either 75 or 330 mm. The short camera length (75 mm) allows to image Z contrast, whereas the long camera length (330 mm) allows simultaneous imaging of Z contrast and diffraction contrast. Bright-field images were digitally recorded. Semi-quantitative compositional spectra on both crystalline and amorphous phases were obtained from EDX spectrometer within 60-120 s live time. Beam size in scanning transmission electron mode was 1 to 2 nm and applied across the preselected areas during data acquisition. Structural information on crystalline phases was obtained from selected area electron diffraction patterns recorded on image plates for high precision.

2.9 Fe isotope analysis

Vivianite mineral separates were processed for Fe isotope analyses at the HELGES lab, GFZ Potsdam (von Blanckenburg et al., 2016). Vivianite samples were hand-picked; however, the presence of some minor inclusions of siderite, silicates and oxides could not be ruled out. To avoid dissolution of silicates and oxides, about 5 mg of sample powder was leached with 2M HNO_3 for 24 hours at room temperature (von Blanckenburg et al., 2008). Complete dissolution of vivianite and a few solid residual particles were observed. After centrifugation, supernatants (dissolved vivianite and trace siderite) were evaporated in PFA vials on a hot plate at 110°C, then heated in closed vials at 150 °C with H_2O_2/HNO_3 and aqua regia to remove all OM. Procedure blanks and reference materials (USGS COQ-1 carbonatite rock, BHVO-2 basalt rock, HanFe pure Fe solution) were processed along with samples for quality control. After evaporation, samples were re-dissolved in 6M HCl and an aliquot of ~100 µg Fe was passed through chromatographic columns (DOWEX AG-X8 resin) to purify Fe from other matrix elements (Schoenberg and von Blanckenburg, 2005). Purity and quantitative recovery of Fe was verified by inductively coupled plasma - optical emission spectrometry (ICP-OES, Varian 720ES) and found to be better than 98 %. Cr and Ni were efficiently separated from Fe, thus eliminating spectral interferences of ^{54}Cr on ^{54}Fe and ^{58}Ni on ^{58}Fe. Blanks of all procedures were measured by quadrupole ICP-MS (Thermo iCAP-Qc) and contained <10 ng Fe, thus contributing to <0.01 % of processed Fe samples (~100 µg), and are therefore considered negligible.

https://doi.org/10.5194/bg-2019-426
Preprint. Discussion started: 14 November 2019

Prior to isotope analysis, samples were dissolved in 0.3 M HNO_3 and diluted to ~5 µg mL^{-1} Fe to match the concentration of the bracketing standard (IRMM-014) within 10 %. Fe isotopic analyses were performed using a Thermo Scientific Neptune multi-collector inductively coupled plasma mass spectrometer (MC-ICP-MS) equipped with a Neptune Plus Jet Interface pump and a quartz-glass spray chamber (double pass cyclon-scott type, Thermo SIS) with a 100 µL min^{-1} self-aspirating PFA nebulizer for sample introduction. Analyses were run in high mass resolution mode (mass resolving power m/Δm (5 %, 95 %) ~9000) to resolve all Fe isotopes from polyatomic interferences (i.e. ArO, ArOH, and ArN). Potential interferences of ^{54}Cr on ^{54}Fe and ^{58}Ni on ^{58}Fe were monitored at masses ^{52}Cr and ^{60}Ni. The sample-standard bracketing method (using IRMM-014 as bracketing standard) was used to correct for instrumental mass bias (Schoenberg and von Blanckenburg, 2005). Isotope ratios ($^{56}Fe/^{54}Fe$ and $^{57}Fe/^{54}Fe$) are reported in the δ-notation in per mil (‰) relative to the international reference material IRMM-014 (e.g., $\delta^{56}Fe = (^{56}Fe/^{54}Fe_{sample}/^{56}Fe/^{54}Fe_{IRMM\text{-}04} - 1) \times 1000$). Measurements were repeated between 2 and 8 times in two independent analytical sessions. Results of $\delta^{57}Fe$ and $\delta^{56}Fe$ all follow mass-dependent isotope fractionation and therefore results are only discussed in terms of $\delta^{56}Fe$ with an uncertainty of the method estimated to be ± 0.05 ‰ (2σ) in $\delta^{56}Fe$, as verified during this study by repeated analyses of reference materials and comparison to published reference values (Supplementary Table S1).

3 Results

3.1 Lithology and core scanning images

The lithology of TDP site 1 is displayed from 0 to 100 m depth (Fig. 2a), ending at the boundary between the predominantly fine-grained lacustrine Unit 1 and the more coarse-grained fluvio-lacustrine Unit 2 (Russell et al., 2016). The upper 100 m of sediment consist largely of alternating dark reddish-grey and brown to dark-green grey lacustrine clay beds (Fig. 2a-b). Turbidites are relatively rare but more common below 50 m and above 25 m depth and two ~5 m beds of diatom ooze occur at ~35 and 45 m depth. We also observed tephras throughout Unit 1. We focus on 5 intervals containing vivianites between 20 and 50 m depth, where sediment types include both red and green clays, diatomaceous oozes and several large tephras (Fig. 2a). Vivianites are mostly found in green clays, often overlain by siderite-rich red clays and, occasionally, turbidites (Supplementary Fig. S3). Diatomaceous oozes are devoid of vivianite and siderite. A more detailed description of the full stratigraphy is published elsewhere (Russell et al., 2016).

3.2 Total organic carbon and total iron

Over the upper 100 m of the sediment sequence at site TDP-1A, TOC values (Fig. 2a) vary between ~6 and 0.2 wt %. The upper 20 m of sediments display concentrations fluctuating between 3.5 and 0.5 wt % with an overall decrease with depth. In the vivianite-bearing interval (20-50 m), values reach maxima of ~3 wt % in the diatomaceous oozes. In the lowermost part

https://doi.org/10.5194/bg-2019-426
Preprint. Discussion started: 14 November 2019

of the record, TOC gradually increases from 1.0 wt % at 50 m depth to 4.0 wt % at 80 m depth, with highest values (~6%) at the bottom of the core just above the peat layer.

Total iron concentrations generally fluctuate between 15 and 20 wt % in Unit 1, with the exception of the interval between 50 and 80 m depth where values occasionally reach 25 to 30 wt %. Some of these high values occur within turbidite beds. The lowest values (~7 wt %) are found within the diatomaceous oozes at 35 and 45 m depth, and just above a peat layer at ~100 m depth.

3.3 Pore water geochemistry

In the upper 20 m of sediment, pore water DIC concentrations increase gradually from 2 to 6 mM with depth. Values drop to 4 mM at 20 m depth and then increase gradually from 4 to 7 mM down to 100 m depth. Pore water PO_4^{3-} concentrations in the upper 10 m of sediments increase gradually from 0 to 0.62 µM with depth. Between 20 and 50 m depth, values remain low (0.15 to 0.20 µM). Concentrations of pore water Fe^{2+} are highly variable throughout the sedimentary sequence (17-278 µM). Some of the intervals with highest dissolved Fe^{2+} values are found in the uppermost part of the record (1-6 m), from 15-20 m depth just above the vivianite interval, and in the lowermost section of the core (90-100 m). Below 50 m depth, both Fe^{2+} and PO_4^{3-} values generally peak in the vicinity of turbidite layers.

3.4 Iron isotopes

Iron isotopes measured on single vivianite crystals (Fig. 2a) display $\delta^{56}Fe$ values of -0.52 ‰ and -0.44 ‰ at 23 m depth, -0.61 ‰ at 36 m depth, and -0.39 ‰ and -0.46 ‰ at 46 m depth (all ±0.05 ‰, 2 σ). We observe the most negative $\delta^{56}Fe$ values in a specimen from the middle of the vivianite-bearing interval. The iron incorporated in the measured vivianite crystals is isotopically lighter in comparison to the global bulk igneous rock reservoir ($\delta^{56}Fe = +0.1 \pm 0.1$ ‰, e.g. Dauphas et al., 2017 and references therein), which is the value expected for the ultramafic igneous rocks in Lake Towuti's catchment. To the best of our knowledge, there are no existing data on vivianite $\delta^{56}Fe$ in the literature that would allow comparison. As such, Fe isotope fractionation factors remain unknown for vivianite formation. However, previous studies indicate that during Fe redox reactions, the Fe^{2+}-bearing phases generally become enriched in the lighter Fe isotopes compared to Fe^{3+}-bearing phases (e.g., Dauphas et al. 2017). Given that vivianite is a Fe^{2+}-bearing mineral phase, the isotopically light $\delta^{56}Fe$ values we measured in vivianites from Lake Towuti are consistent with the direction of fractionation occurring during Fe^{3+} reduction.

3.5 Vivianite detection, SEM imaging, EDX analysis

The XRD pattern of our powdered vivianite extract confirms identification of this mineral, with an excellent match to reference peaks of one synthetic vivianite from the mineral database (Fig. 3c). Larger vivianite concretions were not observed upon inspection of split core surfaces. Vivianite was also not detected in XRD patterns of bulk sediment at 6

https://doi.org/10.5194/bg-2019-426
Preprint. Discussion started: 14 November 2019

different depths. Siderite, quartz (i.e. SiO_2) and serpentine (i.e. lizardite: $Mg_3Si_2O_5(OH)_4$) were the main minerals clearly identified based on reference peaks in these 6 samples, whereas vivianite was below the XRD detection limit of 1 % (Supplementary Fig. S2).

SEM images of single vivianite crystals (Fig. 3a) show that the habit varies from tabular crystals at 23 m depth to rosette at 36 m depth with addition of blades and overall growth at 46 m depth, and the largest crystal (>7 cm) being found at 50 m depth. EDX points of analysis indicate partial substitution of Fe^{2+} by Mn^{2+} in the structure of vivianite crystals from 23 and 36 m depth (up to ~17% Fe substitution), resulting in their overall "manganoan" composition (Fig. 3b). Such compositions have been previously reported from both freshwater and marine sediments although with variable Mn concentrations (Fagel et al., 2005; Dijkstra et al., 2016). High Fe content outside the stoichiometric range of vivianite indicates the presence of residual oxides within the crystals. SEM images with location of all EDX points of analysis are available as supplement (Supplementary Fig. S4).

3.6 EDX elemental mapping, TEM imaging

SEM images of the vivianite thin section in back-scattering electron mode reveal a central tabular crystal and imply growth of subsequent blades with preferential orientation directed towards the sediment surface (Fig. 4a). Close-ups also reveal the presence of mineral inclusions entrapped within the central tabular blade and upper side of the vivianite (Fig. 4a), namely siderite (1), millerite (2) and goethite (3). Siderite appears in the form of aggregated nanocrystals, millerite in a micro-acicular habit forming radiating aggregates, and goethite in irregular sheets whose jagged edges and dissolution features likely indicate a detrital origin and potentially partial sedimentary dissolution from iron reduction. EDX elemental mapping (Fig. 4b) as well as individual analyses (Fig. 4c) confirms the composition and identity of these inclusions. Increased intensities of Fe and Mn correspond to goethite, S and Ni to millerite, while those of Si and Al indicate the presence of phyllosilicates inside and between vivianite blades. Ternary diagrams for individual EDX analyses show that millerite incorporates traces of iron, whereas traces of Mn in iron oxides indicates goethite rather than hematite in which Fe substitution by Mn is limited (Singh et al., 2000).

Scanning TEM imaging of Z contrast and diffraction contrast (i.e. 330 mm) show that the vivianite sample from 46.8 m depth has a denser structure than the one from 36.7 m depth. Close-up images reveal the presence of iron oxides (a), illite clays (b) and detrital pyroxene (c), as confirmed by their EDX analyses, which show that vivianite incorporates phases of detrital origin. Fractures in the crystal from 36.7 m depth could be due to its partial oxidation and dehydration (Hanzel et al., 1990), or to immaturity relative to the sample from 46.8 m depth. Finally, the high resolution electron diffraction pattern of the deepest (oldest) vivianite sample from 46.8 m depth demonstrates its well-ordered monoclinic structure (d), whereas the pattern of the one from 36.7 m depth is somewhat kinked.

https://doi.org/10.5194/bg-2019-426
Preprint. Discussion started: 14 November 2019

4 Discussion

4.1 Early microbial diagenesis and vivianite growth

The formation of vivianite in sediments often results from small-scale microbially mediated reactions (Rothe et al., 2016), such as reduction of ferric Fe minerals, with partial dissolution and/or precipitation of mineral phases (Rothe et al., 2014; Egger et al., 2015; Tamuntuan et al., 2015; Dijkstra et al., 2016), alongside OM decomposition (Gächter et al., 2003; Hupfer and Lewandowski, 2008). The ferrous Fe and P released from these reactions may produce vivianite, and/or be consumed through reactions with other dissolved elements such as S. In Fe-rich, oligotrophic settings like Lake Towuti and Lake Matano where HS^- is minimal (Vuillemin et al., 2016), the first authigenic Fe minerals expected to form via the reduction of ferrihydrite are mixed-valence iron oxides (e.g. green rust, magnetite) rather than sulfides (Crowe et al., 2008; Zegeye et al., 2012; Vuillemin et al., 2019a). In nearby Lake Matano, lake waters contain more than 40 nM Ni and are supersaturated with respect to millerite where sulfide accumulates to low μM concentrations (Crowe et al., 2008). By analogy to Lake Matano, Ni would compete with Fe for sulfide in Lake Towuti and its sediments. Indeed, we observed the presence of authigenic millerite in the sediment (Fig. 4) which forms due to the preferential reaction of H_2S with dissolved Ni^{2+} instead of Fe^{2+} (Ferris et al., 1987). Because rates of sulfide production are so low compared to the Fe delivery flux and because Ni is abundant, HS^- has a negligible effect on P release from the sediment. Similarly, in sediments such as Lake Towuti's, siderite is an expected mineral phase, and indeed siderite is abundant in some of Towuti's sediments (Ordoñez et al., 2019; Vuillemin et al., 2019a), implying that CO_3^{2-} can compete with PO_4^{3-} for available Fe.

We observed an apparent progression in vivianite morphology from tabular to rosette with increasing depth down core (Figs. 3a and Supplementary Fig. S4). Vivianite crystals develop radially and vertically during diagenesis, incorporating authigenic phases and detrital silicates within the crystal and between blades (Figs. 4-5, and Supplementary Fig. S5). Authigenic phases (e.g. siderite, millerite) and detrital oxides (e.g. goethite) were trapped within these crystals (Fig. 4a). Millerite is mainly observed in the tabular template, whereas siderite and goethite are found in the upper blades of the crystal (Figs. 4a-4b). The fact that authigenic siderite and millerite are observed within vivianite crystals demonstrates that vivianite forms at a later stage of diagenesis. Vivianite crystals display growth orientation toward the sediment surface, as shown by the development of successive rosettes on site (Supplementary Fig. S5). In pelagic fine sediments, crystals build up to form successive spherules stacked on top of each other reaching sizes of ~4 to 7 cm (Supplementary Figs. S3 and S5).

Because of the high concentrations of Fe oxides in Lake Towuti's sediment (~ 20 wt %), it is very unlikely that much P could escape to the bottom water. Today, iron oxides persist in sediment even with full anoxia at the water-sediment interface. Moreover, whole-lake Fe, P and oxygen dynamics predict that any P that might escape to the photic zone from deep, anoxic settings can be buried in shallow-water, oxidizing sediments. In the deep sediments, pore water PO_4^{3-} concentrations are constantly low in the interval where vivianite crystals are observed (Fig. 2a), suggesting that vivianites acted as a main P sink during diagenesis (Vuillemin et al., 2013, 2014). Dissolved Fe^{2+} concentrations are not particularly low and fluctuate (40-100 μM), suggesting excess Fe relative to P and potentially reflecting dissolution of detrital phases

https://doi.org/10.5194/bg-2019-426
Preprint. Discussion started: 14 November 2019

(e.g. ferrihydrite, goethite, hematite) and/or precipitation of authigenic ones (e.g. magnetite, siderite, vivianite). Concentrations of DIC, which is produced during OM degradation, gradually increase with depth but remain rather constant (4 mM) in the vivianite-bearing intervals, suggesting that PO_4^{3-} can outcompete CO_3^{2-} for available Fe if DIC is used by autotrophic microbes during methane production, thereby leading to vivianite formation under methanogenic settings (Reed et al., 2011; Dijkstra et al., 2016). The fact that dissolved PO_4^{3-}, Fe^{2+} and DIC vary independently also implies a decoupling in their production and consumption rates (e.g. through mineral formation and microbial metabolic consumption), such that they are not simply linked through steady-state OM respiration coupled to Fe reduction and are rather subject to variety of processes that are variable down core.

4.2 Lacustrine conditions promoting vivianite formation

In sulfur-poor, ferruginous settings, vivianite, siderite and magnetite can be formed in the sediments (Potsma, 1981) depending on the local pH, CO_2, PO_4^{3-}, and the amount of reactive ferric oxides buried in the sediment (Fredrickson et al., 1998; Glasauer et al., 2003; O'Loughlin et al., 2013). In shallow sediment cores spanning the last ~60 kyr, Costa et al. (2015) suggested that elevated Fe concentrations represent time intervals of enhanced lake mixing. The alternating dark reddish-brown and lighter green/grey beds, in which vivianites were found in the deeper TDP cores (Fig. 2b, Supplementary Fig. S3), also suggest that variable oxygenation at the water-sediment interface in the past (Costa et al., 2015; Russell et al., 2016). Some vivianite-bearing beds appear at similar locations in multiple holes, suggesting lake-wide chemical conditions promoted subsequent growth of vivianite in the sediment (Supplementary Fig. S4). However, in other cases, vivianites appear sporadically in only one core. Below the layer in which the biggest vivianite crystal (>7 cm) was found (~50 m sediment depth), we observe increased iron concentrations (>30 %) corresponding to siderite-rich sediments and multiple turbidites (~50 to 60 m; Fig. 2a). Sporadic turbidites could result in discrete layers enriched in siderites, which are sometimes also linked to bottom water oxygenation, due to enhanced deposition of iron oxides and precipitation of HCO_3^- and Fe^{2+} shortly after deposition (Hasberg et al., 2019; Sheppard et al., 2019). Such turbidites may also promote sporadic laterally non-contiguous vivianite formation in one site (Supplementary Fig. S4). For instance, a large flat-topped vivianite crystal (>4 cm) capped by a turbidite shows how rapid sedimentary processes prevent further growth of this mineral (Supplementary Fig. S5).

Within the vivianite-bearing interval (20-50 m depth), diatomaceous oozes signify relatively high primary productivity, and their corresponding iron concentrations are lowest, which is consistent with the absence of siderite and vivianite therein (Fig. 2a). The presence of diatomaceous oozes, with vivianites below and above these sediments, indicates that P concentrations in the water column were much higher during this time interval compared to present-day levels, pointing either to increased P supply to the basin and/or a change in P recycling. Given the slow sedimentation rates (~0.2 m kyr^{-1}) in the upper 10 m of sediments (Russell et al., 2014), it seems likely that the 20-50 m interval encompasses at least 100 kyrs. During the Last Glacial Maximum (LGM), Towuti's lake level was 15 to 30 m lower than today, possibly resulting in endorheic conditions (Costa et al., 2015; Vogel et al., 2015). By analogy, lake levels may have been lower during preceding glacial phases, at least

https://doi.org/10.5194/bg-2019-426
Preprint. Discussion started: 14 November 2019

one of which is likely to be included in the vivianite-bearing interval (Fig. 2). While lake shrinkage could affect algal productivity in the remaining waters (Clavero et al., 1993; Schütt, 1998; Bernal-Brooks et al., 2003; Recasens et al., 2015), lower lake levels should promote bottom water oxygenation and burial of Fe-oxides, and thereby suppress P recycling. Tephras could represent an additional source of P to the lake if they bear apatite (i.e. $Ca_5(PO_4)_3$ (OH)) or additional P adsorbed onto their mineral phases (Harper et al., 1986; Nanzyo et al., 1997; Ayris and Delmelle, 2012). Moreover, sediment-starved conditions would limit P scavenging in the water column. In contrast, increased delivery of detrital iron (oxyhydr)oxides precipitates P to the sediment and initially forms sideritic beds, whereas vivianite formation initiates under slow kinetics deeper in the sediment than for siderite (Potsma, 1981) as demonstrated by the incorporation of siderite, millerite and clay minerals in the vivianites (Figs. 4 and 5).

4.3 δ^{56}Fe compositions of vivianites

Dissimilatory microbial reduction of iron releases Fe^{2+} in pore water that is up to 2 ‰ lighter than the original substrates (Crosby et al., 2007; Tangalos et al., 2010), therefore iron isotopes can be used to trace redox processes related to microbial activity in aquatic sediments (Song et al., 2011; Percak-Dennett et al., 2013; Busigny et al., 2014; Liu et al., 2015). During early diagenesis, the preferential dissolution of isotopically light Fe^{2+} leaves behind an increasingly heavier residual Fe pool (Staubwasser et al., 2006), which results in the diffusive accumulation of the light isotopes in the top layer of sediments where they can be adsorbed and incorporated into ferrous Fe phases. The δ^{56}Fe values reported for pore water Fe^{2+} in lacustrine sediments range between -2 and -1 ‰ and become heavier with depth as authigenic phases form (Song et al. 2011; Percak-Denett et al. 2013). The δ^{56}Fe values for reduced Fe phases formed in the sediment are highly variable and range from -1.5 to -0.8 ‰ for pyrite (Busigny et al., 2014), -1.6 to 0.3 ‰ for siderite (Johnson et al., 2005) and -0.1 to 0.2 ‰ for magnetite (Percak-Denett et al. 2013). The δ^{56}Fe measured on whole vivianite crystals (-0.61 to -0.39 ‰) reveals incorporation of isotopically fractionated light Fe^{2+} (Fig. 2a), which are quite different from the positive δ^{56}Fe values expected for detrital iron-bearing minerals or secondary oxides (Staubwasser et al., 2006; Severmann et al., 2008; Liu et al. 2015). We observe these depleted δ^{56}Fe even though traces of detrital iron-bearing minerals and secondary oxides are present within vivianite crystals (Figs 4 and 5). Because of these light vivianite δ^{56}Fe values (Fig. 2), we propose that vivianite acted as an additional trap for the microbially reduced Fe^{2+} in pore water (Bullen et al., 2001; Wu et al. 2011). This is also consistent with the lower siderite content of these sediments, which would rather be selected for under increased delivery of detrital iron (oxyhydr)oxides to the sediment (Fredrickson et al., 1998; Glasauer et al., 2003; O'Loughlin et al., 2013).

https://doi.org/10.5194/bg-2019-426
Preprint. Discussion started: 14 November 2019

5. Conclusions

Non-steady state conditions likely promoted the sporadic formation of diagenetic vivianites within otherwise siderite-rich sediments during a prolonged interval of ferruginous Lake Towuti's history. Although the source of P is not well constrained, its inputs stimulated diatom productivity and sporadic vivianite formation during diagenesis. Inclusions of millerite, siderite and partially dissolved iron oxides within vivianite crystals support the assumption that microbial iron and SO_4^{2-} reduction took place prior to vivianite formation. With depth and over time, vivianite crystals grew and changed from tabular to rosette morphologies, including surrounding clays. The corresponding $\delta^{56}Fe$ compositions confirmed that these crystals incorporated microbially fractionated light Fe^{2+} during diagenesis, while their lightest isotopic signature may also point to pre-depositional Fe fractionation related to lake mixing. Although crystallization time was not constrained, supply of pore water PO_4^{3-} and Fe^{2+} during diagenesis maintained saturation with respect to vivianite and supported the continuous growth of crystals with depth.

Data availability

Present scientific data are archived and publicly available at PANGAEA® Data Publisher for Earth & Environmental Science (Vuillemin et al., 2019b).

Author contributions

AV designed the study, sampled in the field, extracted vivianite crystals, actively took part in SEM, TEM, and XRD analyses, designed the figures and led the writing of the present manuscript. AF sampled in the field and measured pore water geochemistry. RW operated the TEM. JAS and FvB processed and measured iron isotopes. AMS led XRD analyses. HK led SEM analyses. AL led TOC analyses. KWB processed and measured samples for total iron and pore water iron. SN measured pH in the field. RS measured alkalinity in the field. LO sampled in the field and processed cores at LacCore. DA processed and sampled cores at LacCore. CH fulfilled the research permit procedure. As principal investigators of the Towuti Drilling Project, JMR, SB, HV sampled in the field, processed drill core splitting and imaging at LacCore, processed TOC and Fe concentrations on full cores, and supervised the writing of the present manuscript. SAC sampled in the field, fulfilled the research permit procedure, supervised iron analyses and writing of the present manuscript. JK sampled in the field and at LacCore, supervised geochemical analyses and writing of the present manuscript. The Towuti Drilling Project Science Team actively participated in drilling operations and processing of the cores at LacCore.

https://doi.org/10.5194/bg-2019-426
Preprint. Discussion started: 14 November 2019

Competing interests

The authors declare that they have no conflict of interest.

Acknowledgements

This research was carried out with partial support from the International Continental Scientific Drilling Program (ICDP), the U.S. National Science Foundation (NSF), the German Research Foundation (DFG), the Swiss National Science Foundation (SNSF), PT Vale Indonesia, the Ministry of Research, Education, and Higher Technology of Indonesia (RISTEK), Brown University, the University of Minnesota, the University of Geneva, GFZ German Research Centre for Geosciences, the Natural Sciences and Engineering Research Council of Canada (NSERC), and Genome British Columbia. This study was financially and logistically supported by the DFG ICDP priority program through grants to JK (KA 2293/8-1) and AV (VU 94/1-1), an SNSF grant to AV (P2GEP2_148621) and an NSERC Discovery grant (0487) to SAC.

We thank PT Vale Indonesia, the U.S. Continental Scientific Drilling and Coordination Office, and U.S. National Lacustrine Core Repository, and DOSECC Exploration Services for logistical support. The research was carried out with permissions from RISTEK, the Ministry of Trade of the Republic of Indonesia, the Natural Resources Conservation Center (BKSDA), and the Government of Luwu Timur of Sulawesi. We thank the Director of the Indonesia Research Center for Limnology (P2L) - Indonesian Institute of Sciences (LIPI), Tri Widiyanto and his staff of P2L-LIPI for their administrative support in obtaining the Scientific Research Permit. Supervision by the scientific crew of LacCore during core splitting and subsampling is kindly acknowledged. We also thank Aan Diyanto, Axel J. Kitte, Anja Schreiber, Ilona Schäpan and Johannes Glodny for their assistance during field sampling, TEM and SEM analyses and mineral extractions, respectively.

Team members

Other members of the TDP Science Team are M. Melles, S. Fajar, A. Hafidz, D. Haffner, A. Hasberg, S. Ivory, C. Kelly, J. King, K. Kirana, M. Morlock, A. Noren, R. O'Grady, J. Stevenson, T. von Rintelen, I. Watkinson, N. Wattrus, S. Wicaksono, T. Wonik, A. Deino, A. M. Imran, R. Marwoto, L. O. Ngkoimani, L. O. Safiuddin, and G. Tamuntuan.

References

Ayris, P. M., and Delmelle, P.: The direct environmental effects of tephra emission, Bull. Volcanol., 74, 1905-1936, https://doi.org/10.1007/s00445-012-0654-5, 2012.

https://doi.org/10.5194/bg-2019-426
Preprint. Discussion started: 14 November 2019

Beard, B. L., Handler, R. M., Scherer, M. M., Wu, L., Czaja, A. D., Heimann, A., and Johnson, C. M.: Iron isotope fractionation between aqueous ferrous iron and goethite, Earth Planet. Sc. Lett., 295, 241-250, https://doi.org/10.1016/j.epsl.2010.04.006, 2010.

Bernal-Brooks, F. W., Dávalos-Lind, L., and Lind, O. T.: Seasonal and spatial variation in algal growth potential and growth-limiting nutrients in a shallow endorheic lake: Lake Pátzcuaro (Mexico), Lakes Reserv. Res. Manag. 8, 83-93, https://doi.org/10.1046/j.1320-5331.2003.00217.x, 2003.

Bramburger, A. J., Hamilton, P. B., Hehanussa, P. E., and Haffner, G. D.: Processes regulating the community composition and relative abundance of taxa in the diatom communities of the Malili Lakes, Sulawesi Island, Indonesia, Hydrobiologia, 615, 215–224, https://doi.org/10.1007/s10750-008-9562-2, 2008.

Bullen, T. D., White, A. F., Childs, C. W., Vivit, D. V., and Schulz M. S.: Demonstration of significant abiotic iron isotope fractionation in nature, Geology, 29, 699-702, https://doi.org/10.1130/0091-7613(2001)029<0699:DOSAII>2.0.CO;2, 2001.

Busigny, V., Planavsky, N. J., Jézéquel, D., Crowe, S., Louvat, P., Moureau, J., Viollier, E., and Lyons, T. W.: Iron isotopes in an Archean ocean analogue, Geochim. Cosmochim. Ac., 133, 443-462, https://doi.org/10.1016/j.gca.2014.03.004, 2014.

Clavero, V., Garcia, M., Fernández, J. A., and Niell, F. X.: Adsorption-desorption of phosphate and its availability in the sediment of a saline lake (Fuente de Piedra, southern Spain), Int. J. Salt Lake Res. 2, 153-163, https://doi.org/10.10007/BF02905907, 1993.

Compton, J., Mallinson, D., Glenn, C. R., Filippelli, G., Föllmi, K., Shields, G., and Zanin, Y.: Variations in the global phosphorus cycle. SEPM Spec. P., 66, 21-33, https://doi.org/10.2110/pec.00.66.0021, 2010.

Costa, K. M., Russell, J. M., Vogel, H., and Bijaksana, S.: Hydrological connectivity and mixing of Lake Towuti, Indonesia, in response to paleoclimatic changes over the last 60,000 years, Palaeogeogr. Palaeocl., 417, 467-475, https://doi.org/10.1016/j.palaeo.2014.10.009, 2015.

Crosby, H. A., Roden, E. E., Johnson C. M., and Beard, B. L.: The mechanisms of iron isotope fractionation produced during dissimilatory Fe(III) reduction by Shewanella putrefaciens and Geobacter sulfurreducens, Geobiology, 5, 169-189, https://doi.org/10.1111/j.1472-4669.2007.00103.x, 2007.

Crowe, S. A., Pannalal, S. J., Fowle, D. A., Cioppa, M. T., Symons, D. T. A., Haffner, G. D., and Fryer, B. J.: Biogeochemical cycling in Fe-rich sediments from Lake Matano, Indonesia, Int. Symp. Water-Rock Interact., 11, 1185–1189, 2004.

Crowe, S. A., Katsev, S., Hehanussa, P., Haffner, G. D., Sundby, B., Mucci, A., and Fowle, D. A.: The biogeochemistry of tropical lakes: A case study from Lake Matano, Indonesia, Limnol. Oceanogr., 53, 319-331, https://doi.org/10.4319/lo.2008.53.1.0319, 2008.

Dauphas, N., John, S. G., and Rouxel, O.: Iron isotope systematics, Rev. Mineral. Geochem., 82, 415-510, https://doi.org/10.2138/rmg.2017.82.11, 2017.

https://doi.org/10.5194/bg-2019-426
Preprint. Discussion started: 14 November 2019

Dijkstra, N., Slomp, C. P., Behrends, T., and Expedition 347 Scientists: Vivianite is a key sink for phosphorus in sediments of the Landsort Deep, an intermittently anoxic deep basin in the Baltic Sea, Chemic. Geol., 438, 58–72, https://doi.org/10.1016/j.chemgeo.2016.05.025, 2016.

Egger, M., Jilbert, T., Behrends, T., Rivard, C., and Slomp, C. P.: Vivianite is a major sink for phosphorus in methanogenic coastal surface sediments, Geochim. Cosmochim. Ac., 169, 217–235, https://doi.org/10.1016/j.gca.2015.09.012, 2015.

Fagel, N., Alleman, L. Y., Granina, L., Hatert, F., Thamo-Bozso, E., Cloots, R., and Andre, L.: Vivianite formation and distribution in Lake Baikal sediments, Glob. Planet. Change, 46, 315–336, https://doi.org/10.1016/j.gloplacha.2004.09.022, 2005.

Ferris, F. G., Fyfe, W. S., and Beveridge, T. J.: Bacteria as nucleation sites for authigenic minerals in a metal-contaminated lake sediment, Chem. Geol., 63, 252-232, https://doi.org/10.1016/B978-0-444-88900-3.50035-7, 1987.

Fredrickson, J. K., Zachara, J. M., Kennedy, D. W., Dong, H., Onstott, T. C., Hinman, N. W, and Li, S.: Biogenic iron mineralization accompanying the dissimilatory reduction of hydrous ferric oxide by a groundwater bacterium, Geochim. Cosmochim. Ac., 62, 3239 –3257, https://doi.org/10.1016/S0016-7037(98)00243-9, 1998.

Friese, A., Kallmeyer, J. Kitte J. A., Montaño Martinez, I., Bijaksana, S., Wagner, D., the ICDP Lake Chalco Drilling Science Team, and the ICDP Towuti Drilling Science Team: A simple and inexpensive technique for assessing contamination during drilling operations, Limnol. Oceanogr. Methods, 15, 200-211, https://doi.org/10.1002/lom3.10159.

Gächter, R., Meyer, J. S., and Mares, A.: Contribution of bacteria to release and fixation of phosphorus in lake sediments, Limnol. Oceanogr., 33, 1542-1558, https://doi.org/10.4319/lo.1988.33.6_part_2.1542, 1988.

Gächter, R., and Müller, B.: Why the phosphorus retention of lakes does not necessarily depend on the oxygen supply to their sediment surface, Limnol. Oceanogr., 48, 929–933, https://doi.org/10.4319/lo.2003.48.2.0929, 2003.

Glasauer, S., Weidler, P. G., Langley, S., and Beveridge, T. J.: Controls on Fe reduction and mineral formation by a subsurface bacterium, Geochim. Cosmochim. Ac., 67, 1277–1288, https://doi.org/10.1016/S0016-7037(02)01199-7, 2003.

Golightly, J. P.: Progress in understanding the evolution of nickel laterites, in: The Challenge of Finding New Mineral Resources - Global Metallogeny, Innovative Exploration, and New Discoveries, Special Publication 15, Society of Economic Geologists, Denver, United-States, 451–485, 2010.

Golubev, S. V., Bénézeth, P., Schott, J., Dandurand, J. L., and Castillo, A.: Siderite dissolution kinetics in acidic aqueous solutions from 25 to 1000° C and 0 to 50 atm pCO_2, Chem. Geol., 265, 13-19, https://doi.org/10.1016/j.chemgeo.2008.12.031, 2009.

Haffner, G. D., Hehanussa, P. E., and Hartoto, D.: The biology and physical processes of large lakes of Indonesia: Lakes Matano and Towuti, in: The Great Lakes of the World (GLOW): Food-Web, Health, and Integrity, edited by Munawar, M., and Hecky, R.E., Blackhuys, 183-194, 2001.

Hanzel, D., Melsel, W., Hanzel, D., and Gütlich, P.: Mössbauer effect study of the oxidation of vivianite, Solid State Commun., 76, 307-310, https://doi.org/10.1016/0038-1098(90)90843-Z , 1990.

Harper, M., Howorth, R., and McLeod, M.: Late Holocene diatoms in Lake Poukawa: Effects of airfall tephra and changes in depth, New Zeal. J. Mar. Fresh., 20, 107-118, https://doi.org/10.1080/00288330.1986.9516135, 1986.

Hasberg, A. K. M., Bijaksana, S., Held, P., Just, J., Melles, M., Morlock, M. A., Opitz, S., Russell, J. M., Vogel, H., and Wennrich, V.: Modern sedimentation processes in Lake Towuti, Indonesia, revealed by the composition of surface sediments, Sedimentology, 66, 675-698, https://doi.org/10.1111/sed.12503, 2019.

Hupfer, M., and Lewandowski, J.: Oxygen controls the phosphorus release from lake sediments – a long-lasting paradigm in limnology, Int. Rev. Hydrobiol., 93, 415–432, https://doi.org/10.1002/iroh.200711054, 2008.

Johnson, C. M., Roden, E. E., Welch, S. A., Beard, B. L.: Experimental constraints on Fe isotope fractionation during magnetite and Fe carbonate formation coupled to dissimilatory hydrous ferric oxide reduction, Geochem. Cosmochem. Ac., 69, 963-993, https://doi.org/10.1016/j.gca.2004.06.043, 2005.

Johnson, C. A., Murayama, M., Küsel, K., Hochella, M. F. Jr.: Polycrystallinity of green rust minerals and their synthetic analogs: Implications for particle formation and reactivity in complex systems, Am. Mineral., 100, 2091-2105, https://doi.org/10.2138/am-2015-5287, 2015.

Katsev, S., Tsandev, I., L'Heureux, I., and Rancourt, D. G.: Factors controlling long-term phosphorus efflux from lake sediments: Exploratory reactive-transport modeling, Chem. Geol., 234, 127–147, https://doi.org/10.1016/j.chemgeo.2006.05.001, 2006.

Katsev, S., Crowe, S. A., Mucci, A., Sundby, B., Nomosatryo, S., Haffner, G. D., and Fowle, D. A.: Mixing and its effects on biogeochemistry in the persistently stratified, deep, tropical Lake Matano, Indonesia, Limnol. Oceanogr., 55, 763-776, https://doi.org/10.4319/lo.2010.55.2.0763, 2010.

Lehmusluoto, P., Machbub, B., Terangna, N., Rumiputro, S., Achmad, F., Boer, L., Brahmana, S. S., Priadi, B., Setiadji, B., Sayuman, O., Margana, A.: National inventory of the major lakes and reservoirs in Indonesia. General limnology. Expedition Indodanau Technical Report. 1995.

Lemos, V. P., da Costa, M. L., Lemos, R. L., and de Faria, M. S. G.: Vivianite and siderite in lateritic iron crust: an example of bioreduction, Quim. Nova, 30, 36-40, https://doi.org/10.1590/S0100-40422007000100008, 2007.

Manheim, F. T.: A hydraulic squeezer for obtaining interstitial water from consolidated and unconsolidated sediments, USGS Reference Paper, 550, 171–174, 1966.

Liu, K., Wu, L. L., Couture, R. M., Li, W. Q., and Van Cappellen, P.: Iron isotope fractionation in sediments of an oligotrophic freshwater lake, Earth Planet. Sc. Lett., 423, 164-172, https://doi.org/10.1016/j.epsl.2015.05.010, 2015.

Manning, P. G., Murphy, T. P., and Prepas, E. E.: Intensive formation of vivianite in the bottom sediments of mesotrophic Narrow Lake, Alberta, Can. Mineral., 29, 77-85, 1991.

Morlock, M. A., Vogel, H., Nigg, V., Ordoñez, L., Hasberg, A. K. M., Melles, M., Russell, J. M., Bijaksana, S., and the TDP Science Team: Climatic and tectonic controls on source-to-sink processes in the tropical, ultramafic catchment of Lake Towuti, Indonesia, J. Paleolimnol., 61, 279-295, https://doi.org/10.1007/s10933-018-0059-3, 2019.

Nomosatryo, S., Henny, C., Jones, C. A., Michiels, C., and Crowe, S. A.: Karaketristik dan klasifikasi trofik di Danau Matano dan Danau Towuti Sulawesi selatan, Perkembangan Limnologi dalam Mendukung Pembangunan Berkelanjutan di Indonesia: Tantangan dan Harapan, Prosiding Pertemuan Ilmiah Tahunan MLI I, 493-507, 2013.

Nanzyo, M., Takahashi, T., Sato, A., Shoji, S., and Yamada, I: Dilute acid-soluble phosphorus in fresh air-borne tephras and fixation with an increase in active aluminium and iron, Soil Sci. Plant. Nutr., 43, 839-848, https://doi.org/10.1080/00380768.1997.10414650, 1997.

O'Loughlin, E. J., Boyanov, M. I., Flynn, T. M., Gorski, C. A., Hofmann, S. M., McCormick, M. L., Scherer, M. M., and Kemner, K. M.: Effects of bound phosphate on the bioreduction of lepidocrocite (y-FeOOH) and maghemite (y-Fe_2O_3) and formation of secondary minerals, Environ. Sci. Technol., 47, 9157-9166, https://doi.org/10.1021/es400627j, 2013.

Ordoñez, L., Vogel, H., Sebag, D., Ariztegui, D., Adatte, T., Russell, J.M., Kallmeyer, J., Vuillemin, A., Friese, A., Crowe, S.A., Bauer, K.W., Simister, R., Nomosatryo, S., Henny, C., and Bijaksana, S.: Empowering conventional Rock-Eval pyrolysis for organic matter characterization of the siderite-rich sediments of Lake Towuti (Indonesia) using End-Member Analysis. Org. Geochem., 134, 32-44, https://doi.org/10.1016/j.orggeochem.201905.002, 2019.

Percak-Dennett, E. M., Loizeau, J. L., Beard, B. L., Johnson, C. M., and Roden, E. E.: Iron isotope geochemistry of biogenic magnetite-bearing sediments from the Bay of Vidy, Lake Geneva, Chem. Geol., 360, 32-40, https://doi.org/10.1016/j.chemgeo.2013.10.008, 2013.

Potsma, D.: Formation of siderite and vivianite and the pore water composition of a recent bog sediment in Denmark. Chem. Geol., 31, 225-244, https://doi.org/10.1016/0009-2541(80)90088-1, 1981.

Poulton, S. W., and Canfield, D. E.: Development of a sequential extraction procedure for iron: implications for iron partitioning in continentally derived particulates. Chem. Geol., 214, 209-221, https://doi.org/10.1016/j.chemgeo.2004.09.003, 2005.

Prieto, F. J. M., and Millero, F. J.: The values of pK1 + pK2 for the dissociation of carbonic acid in seawater, Geochim. Cosmochim. Ac., 66, 2529–2540, https://doi.org/10.1016/S0016-7037(02)00855-4, 2002.

Recasens, C., Ariztegui, D., Maidana, N. I., Zolitschka, B., and the PASADO Science Team: Diatoms as indicators of hydrological and climatic changes in Laguna Potrok Aike (Patagonia) since the Late Pleistocene, Palaeogeogr. Palaeocl. 417, 309-319, https://doi.org/10.1016/j.palaeo.2014.09.021.

Reed, D. C., Slomp, C. P., and Gustafsson, B. G.: Sedimentary phosphorus dynamics and the evolution of bottom-water hypoxia: A coupled benthic-pelagic model of a coastal system, Limnol. Oceanogr., 56, 1075–1092, https://doi.org/10.4319/lo.2011.56.3.1075, 2011.

Reed, D. C., Gustafsson, B. G., and Slomp, C. P.: Shelf-to-basin iron shuttling enhances vivianite formation in deep Baltic Sea sediments, Earth Planet. Sc. Lett., 434, 241-251, https://doi.org/10.1016/j.epsl.2015.11.033, 2016.

Roden, E. E., and Edmonds, J. W.: Phosphate mobilization in iron-rich anaerobic sediments: microbial Fe(III) oxide reduction versus iron-sulfide formation, Arch. Hydrobiol., 139, 347–378, https://doi.org/0003-9136/97/0139-0347, 1997.

Rothe, M., Frederichs, T., Eder, M., Kleeberg, A., and Hupfer, M.: Evidence for vivianite formation and its contribution to long-term phosphorus retention in a recent lake sediment: a novel analytical approach, Biogeosciences, 11, 5169–5180, https://doi.org/10.5194/bg-11-5169-2014, 2014.

Rothe, M., Kleeberg, A., Grüneberg, B., Friese, K., Pérez- Mayo, M., and Hupfer, M.: Sedimentary sulphur:iron ratio indicates vivianite occurrence: A study from two contrasting freshwater systems, PLoS ONE, 10, e0143737, https://doi.org/10.1371/journal.pone.0143737, 2015.

Rothe, M., Kleeberg, A., and Hupfer, M.: The occurrence, identification and environmental relevance of vivianite in waterlogged soils and aquatic sediments, Earth Sci. Rev., 158, 51–64, https://doi.org/10.1016/j.earscirev.2016.04.008, 2016.

Russell, J. M., Vogel, H., Konecky, B. L., Bijaksana, S., Huang, Y., Melles, M., Wattrus, N., Costa, K., and King, J. W.: Glacial forcing of central Indonesian hydroclimate since 60,000 y B.P., P. Natl. Acad. Sci., 111, 5100-5105, https://doi.org/10.1073/pnas.1402373111, 2014.

Russell, J. M., Bijaksana, S., Vogel, H., Melles, M., Kallmeyer, J., Ariztegui, D., Crowe, S., Fajar, S., Hafidz, A., Haffner, D., Hasberg, A., Ivory, S., Kelly, C., King, J., Kirana, K., Morlock, M., Noren, A., O'Grady, R., Ordonez, L., Stevenson, J., von Rintelen, T., Vuillemin, A., Watkinson, I., Wattrus, N., Wicaksono, S., Wonik, T., Bauer, K., Deino, A., Friese, A., Henny, C., Imran, Marwoto, R., Ngkoimani, L. O., Nomosatryo, S., Safiuddin, L. O., Simister, R., and Tamuntuan, G.: The Towuti Drilling Project: Paleoenvironments, biological evolution, and geomicrobiology of a tropical Pacific lake, Sci. Dri., 21, 29–40, https://doi.org/10.5194/sd-21-29-2016, 2016.

Sánchez-Román, M., Puente-Sánchez F., Parro, V., and Amils, R.: Nucleation of Fe-rich phosphate and carbonate on microbial cells and exoplymeric substances. Front. Microbiol., 6, 1024, https://doi.org/10.3389/fmicb.2015.01024, 2015.

Sapota, T., Aldahan, A., and Al-Aasm, I. S.: Sedimentary facies and climate control of formation of vivianite and siderite microconcretions in sediments of Lake Baikal, Siberia, J. Paleolimnol., 36, 245–257, https://doi.org/10.1007/s10933-006-9005-x, 2006.

Schoenberg, R., and von Blanckenburg, F.: An assessment of the accuracy of stable Fe isotope ratio measurements on samples with organic and inorganic matrices by high-resolution multicollector ICP-MS, Int. J. Mass Spectrom., 242, 257-272, https://doi.org/10.1016/j.ijms.2004.11.025, 2005.

Shaffer, G.: Phosphate pumps and shuttles in the Black Sea. Nature 321, 515-517. https://doi.org/10.1038/321515a0.

Sheppard, R. Y., Milliken, R. E., Russell, J. M., Darby Dyar, M., Sklute, E. C., Vogel, H., Melles, M., Bijaksana, S., Morlock, M. A., and Hasberg, A. K. M.: Characterization of iron in Lake Towuti sediment. Chem. Geol. 512, 11-30. https://doi.org/10.1016/j.chemgeo.2019.02.029, 2019.

Schütt, B.: Reconstruction of Holocene paleoenvironments in the endorheic basin of Laguna de Gallocanta, Central Spain by investigation of mineralogical and geochemical characters from lacustrine sediments J. Paleolimnol. 20, 217-234, https://doi.org/10-1023/A:1007924000636, 1998.

https://doi.org/10.5194/bg-2019-426
Preprint. Discussion started: 14 November 2019

Singh, B., Sherman, D. M., Gilkes, R. J., Wells, M., and Mosselmans, J. F. W.: Structural chemistry of Fe, Mn, and Ni in synthetic hematites as determined by extended X-ray absorption fine structure spectroscopy, Clay Clay Miner., 48, 521-527, https://doi.org/10.1346/CCMN.2000.0480504, 2000.

Song, L. T., Liu, C., Wang, Z., Zhu, X., Teng, Y., Wang, J., Tang, S., Li, J., and Liang, L.: Iron isotope compositions of natural river and lake samples in the karst area, Guizhou Province, Southwest China, Acta Geol. Sin.-Engl., 85, 712-722, https://doi.org/10.1111/j.1755-6724.2011.00464.x, 2011.

Stamatakis, M. G., and Koukouzas, N. K.: The occurrence of phosphate minerals in lacustrine clayey diatomite deposits, Thessaly, Central Greece, Sediment. Geol., 139, 33–47, https://doi.org/10.1016/S0037-0738(00)00154-8, 2001.

Staubwasser, M., von Blanckenburg, F., and Schoenberg, R.: Iron isotopes in the early marine diagenetic iron cycle, Geology, 34, 629-632, https://doi.org/10.1130/622647.1, 2006.

Tamuntuan, G., Bijaksana, S., King, J., Russell, J., Fauzi, U., and Maryunani, K.: Variation of magnetic properties in sediments from Lake Towuti, Indoensia, and its paleoclimatic significance, Palaeogeogr. Palaeoclimatol. Palaeoecol., 420, 163–172, https://doi.org/10.1016/j.palaeo.2014.12.008, 2015.

Tangalos, G. E., Beard, B. L., and Johnson, C. M.: Microbial production of isotopically light iron(II) in a modern chemically precipitated sediment and implications for isotopic variations in ancient rocks, Geobiology, 8, 197-208, https://doi.org/10.1111/j.1472-4669.2010.00237.x, 2010.

Trolard, F., Bourrié, G., Abdelmoula, M., Refait, P., and Feder, F.: Fougèrite, a new mineral of the pyroaurite-iowaite group: Description and crystal structure, Clay Clay Miner., 55, 323-334, https://doi.org/10.1346/CCMN.2007.0550308, 2007.

Vogel, H., Russell, J. M., Cahyarini, S. Y., Bijaksana, S., Wattrus, N., Rethemeyer, J., and Melles, M.: Depositional modes and lake-level variability at Lake Towuti, Indonesia, during the past ~29 kyr BP, J. Paleolimnol., 54, 359-377, https://doi.org/10.1016/S0883-2927(99)00097-9, 2015.

Viollier, E., Inglett, P. W., Hunter, K., Roychoudhury, A. N., and Van Cappellen P.: The ferrozine method revisited: Fe(II)/Fe(III) determination in natural waters. Appl. Geochem., 15, 785-790, https://doi.org/10.1016/S0883-2927(99)00097-9, 2000.

von Blanckenburg, F., Marnberti, M., Schoenberg, R., Kamber, B. S., and Webb, G. E.: The iron isotope composition of microbial carbonate, Chem. Geol., 249, 113-128, https://doi.org/10.1016/j.chemgeo.2007.12.001, 2008.

von Blanckenburg, F., Wittmann, H., and Schuessler, J. A.: HELGES: Helmholtz Laboratory for the Geochemistry of the Earth Surface. Journal of Large-Scale Research Facilities, 2, https://doi.org/10.17815/jlsrf-2-141, 2016.

Vuillemin, A., Ariztegui, D., Coninck, A., Lücke, A., Mayr, C., Schubert, C., and the PASADO Scientific Team: Origin and significance of diagenetic concretions in sediments of Laguna Potrok Aike, southern Argentina, J. Paleolimnol., 50, 275–291, https://doi.org/10.1007/s10933-013-9723-9, 2013.

Vuillemin, A., Ariztegui, D., Lücke, A., Mayr, C., and the PASADO Science Team: Paleoenvironmental conditions define current sustainability of microbial populations in Laguna Potrok Aike, Argentina, Aquat. Sci., 76, 101-114, https://doi.org/10.1007/s00027-013-0317-4, 2014.

https://doi.org/10.5194/bg-2019-426
Preprint. Discussion started: 14 November 2019

Vuillemin, A., Friese, A., Alawi, M., Henny, C., Nomosatryo, S., Wagner, D., Crowe, S. A., and Kallmeyer, J.: Geomicrobiological features of ferruginous sediments from Lake Towuti, Indonesia, Front. Microbiol., 7, e1007, https://doi.org/10.3389/fmicb.2016.01007, 2016.

Vuillemin, A., Horn, F., Alawi, M., Henny, C., Wagner, D., Crowe, S. A., and Kallmeyer, J.: Preservation and significance of extracellular DNA in ferruginous sediments from Lake Towuti, Indonesia, Front. Microbiol., 8, e1440, https://doi.org/10.3389/fmicb.2017.01440, 2017.

Vuillemin, A., Horn, F., Friese, A., Winkel, M., Alawi, M., Wagner, D., Henny, C., Orsi, W. D., Crowe, S. A., and Kallmeyer, J.: Metabolical potential of microbial communities from ferruginous sediments. Environ. Microbiol., 20, 4297-4313, https://doi.org/10.1111/1462-2920.1443, 2018.

Vuillemin, A., Wirth, R., Kemnitz, H., Schleicher, A.M., Friese, A., Bauer, K.W., Simister, R., Nomosatryo, S., Ordoñez, L., Ariztegui, D., Henny, C., Crowe, S.A., Benning, L.G., Kallmeyer, J., Russell, J.M., Bijaksana, S., Vogel, H., and the Towuti Drilling Project Science Team: Formation of diagenetic siderite in modern ferruginous sediments. Geology 47, 540-544, https://doi.org/ 10.1130/G46100.1, 2019a.

Vuillemin, A., Friese, A., Lücke, A., Bauer, K.W., Nomosatryo, S., Simister, R., Ordoñez, L.G., Ariztegui, D., Russell, J.M., Bijaksana, S., Vogel, H., Crowe, S.A., Kallmeyer, J., and the Towuti Drilling Project Science Team: Pore water geochemistry and bulk sediment measurements of downcore profiles from site TDP-1A of the ICDP Towuti Drilling Project, Lake Towuti, Indonesia. Dataset #908080, doi: 10.1594/PANGAEA.908080, 2019b.

Wilson, T. A., Amirbahman, A., Norton, S. A., and Voytek, M. A.: A record of phosphorus dynamics in oligotrophic lake sediment, J. Paleolimnol., 44, 279-294, https://doi.org/10.1007/s10933-009-9403-y, 2010.

Wirth, R.: Focused Ion Beam (FIB) combined with SEM and TEM: Advanced analytical tools for studies of chemical composition, microstructure and crystal structure in geomaterials on a nanometre scale, Chem. Geol., 261, 217-229, https://doi.org/10.1016/j.chemgeo.2008.05.019, 2009.

Wu, L. L., Beard, B. L., Roden, E. E., and Johnson, C. M.: Stable iron isotope fractionation between aqueous Fe(II) and hydrous ferric oxide, Environ. Sci. Technol. 45, 1847-1852, https://doi.org/10.1021/es103171x, 2011.

Zachara, J. M., Fredrickson, J. K., Li, S. M., Kennedy, D. W., Smith, S. C., and Gassman, P. L.: Bacterial reduction of crystalline Fe^{3+} oxides in single phase suspensions and subsurface materials, Am. Miner., 83, 1426-1443, https://doi.org/10.2138/am-1998-1105, 1998.

Zegeye, A., Bonneville, S., Benning, L. G., Sturm, A., Fowle, D. A., Jones, C., Canfield, D. E., Ruby, C., MacLean, L. C., Nomosatryo, S., Crowe, S. A., and Poulton, S. W.: Green rust formation controls nutrient availability in a ferruginous water column, Geology, 40, 599-602, https://doi.org/10.1130/G32959.1, 2012.

Figures

https://doi.org/10.5194/bg-2019-426
Preprint. Discussion started: 14 November 2019

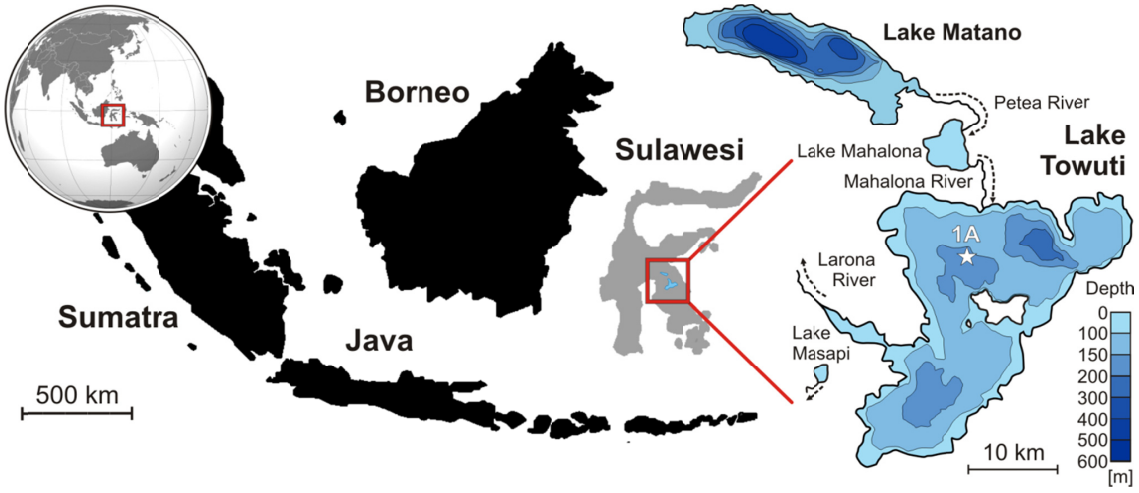

Figure 1: Location of the Malili Lake System and bathymetric map of Lake Matano and Towuti. (**Left**) World map displaying the location of Sulawesi Island (red square) with close-up on the Indonesia archipelago and location of the Malili Lake System (red square). (**Right**) Bathymetric map of Lake Matano and Lake Towuti with position of the ICDP drilling site TDP-1A from which hydraulic piston cores were retrieved and sampled for this study.

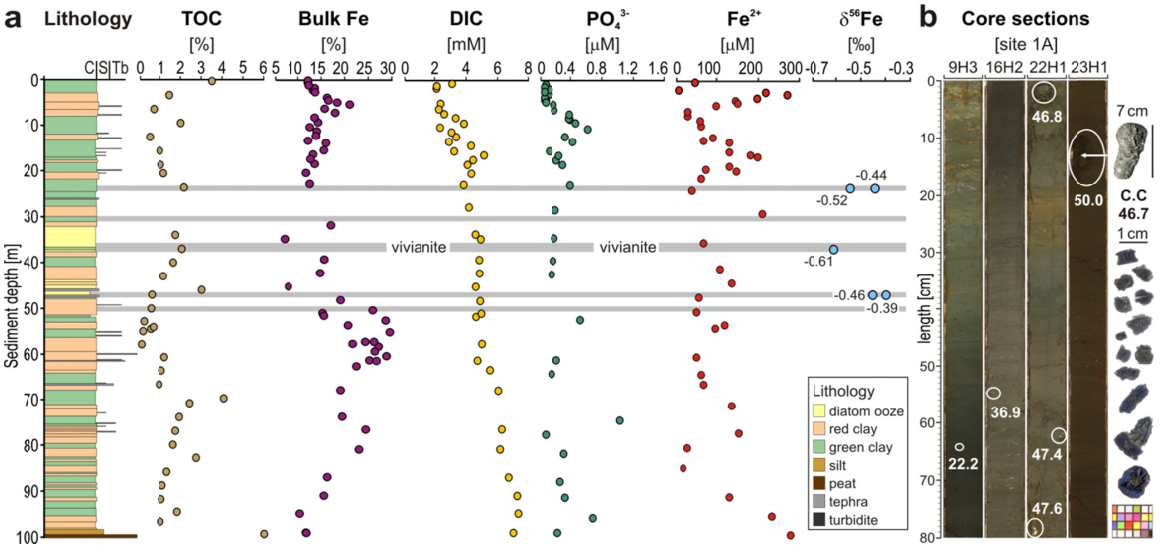

Figure 2: Stratigraphy of composite site TDP-1, multiple profiles established on sediment core subsamples, and core section images. (**a**) Stratigraphy of composite site TDP-1 (after Russell et al., 2016) and corresponding grain sizes (C: clay; S: silt; Tb: turbidite); total organic carbon (TOC), total iron [weight %] in bulk sediment; dissolved inorganic carbon (DIC) [mM], phosphate and iron concentrations [µM] measured in pore water; and δ^{56}Fe isotopic compositions of vivianite crystals. (**b**) Images of core sections from which vivianite crystals were hand-picked. Crystals on the far right were extracted from core catchers.

https://doi.org/10.5194/bg-2019-426
Preprint. Discussion started: 14 November 2019

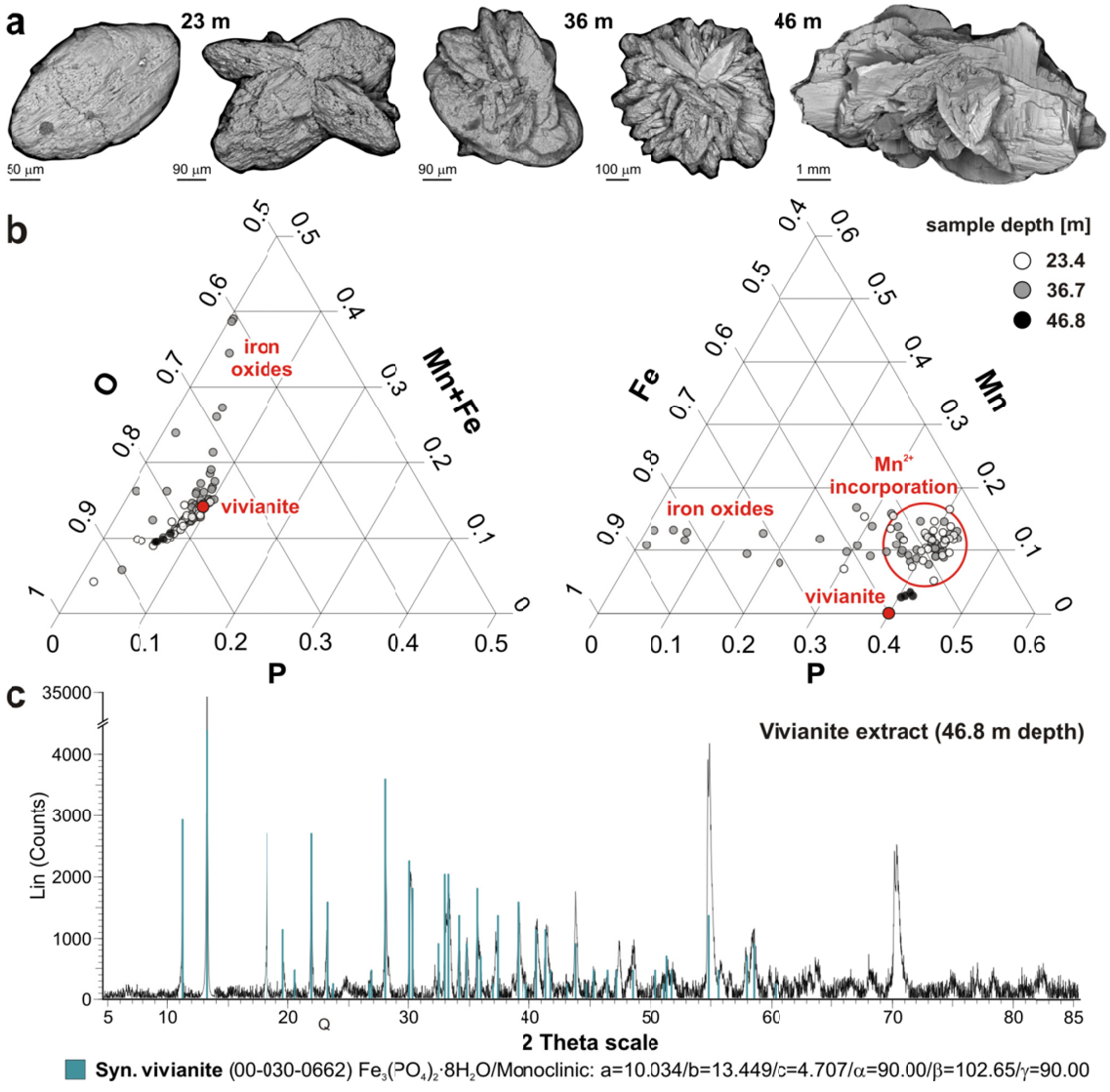

Figure 3: SEM images of vivianite crystals, ternary diagrams of EDX punctual analyses and XRD spectrum. (**a**) SEM images show that vivianite crystals grow from a tabular habit to rosette. (**b**) EDX elemental analyses (i.e. O, P, Fe, Mn) of vivianite crystals standardized to 100 % for each ternary diagram. Results indicate incorporation of manganese in the vivianites with the presence of detrital iron oxides. Deepest samples plot closer to stoichiometric vivianite (red dot). (**c**) XRD spectrum of pure vivianite extract from 46.8 m depth with reference peaks of synthetic vivianite (blue bars).

https://doi.org/10.5194/bg-2019-426
Preprint. Discussion started: 14 November 2019

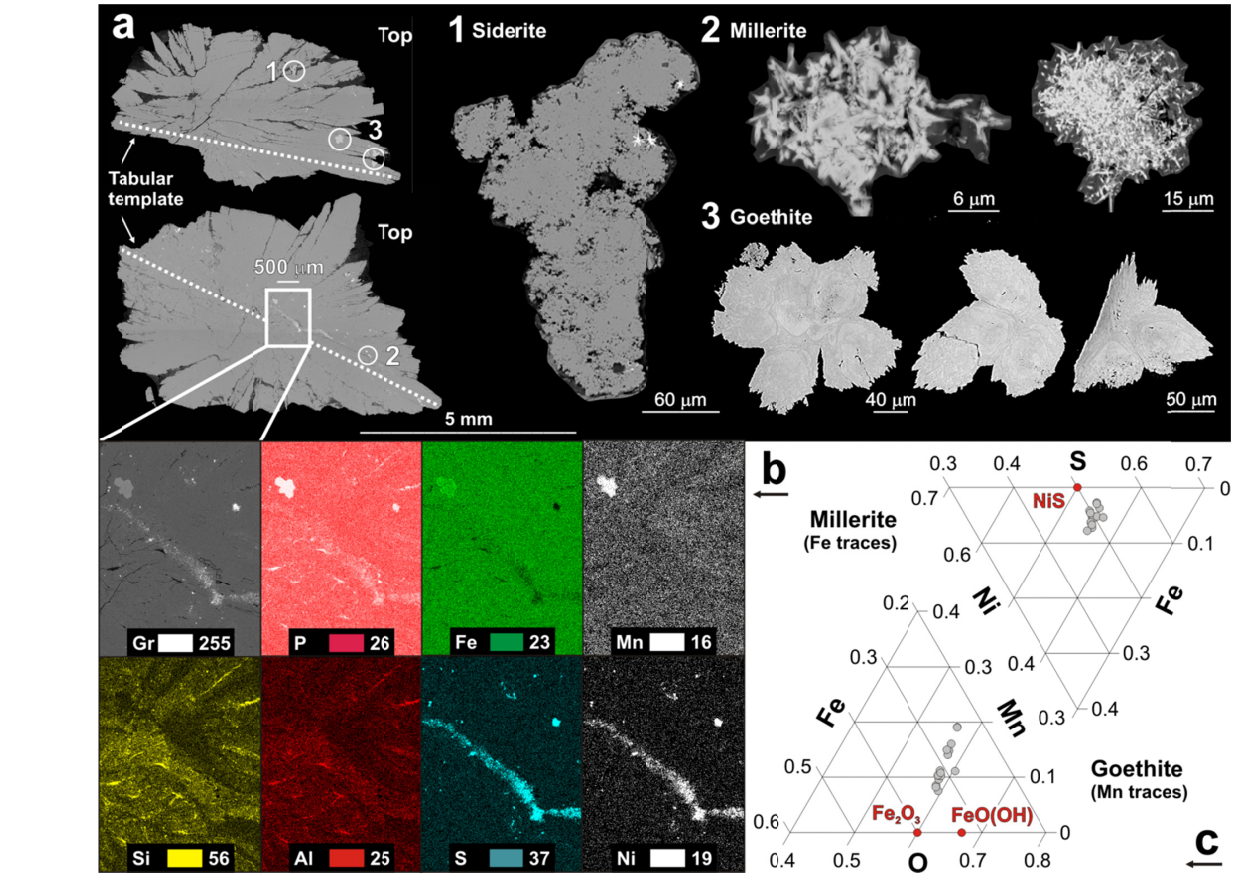

Figure 4: SEM images of vivianite crystal in axial section, and close-ups to mineral inclusions with EDX mapping and punctual analyses. (**a**) SEM images of an axial section of a vivianite crystal from 46.8 m depth, with inclusions of siderite (1), millerite (2) and goethite (3). (**b**) EDX elemental mapping of the framed area with relative intensity images for grey levels (Gr), phosphorus (P), iron (Fe), manganese (Mn), silicium (Si), aluminium (Al), sulfur (S) and nickel (Ni). (**c**) Ternary diagrams displaying the elemental composition of millerite and goethite as measured by punctual EDX analyses. Millerite and goethite crystals contain traces of iron and manganese, respectively.

https://doi.org/10.5194/bg-2019-426
Preprint. Discussion started: 14 November 2019

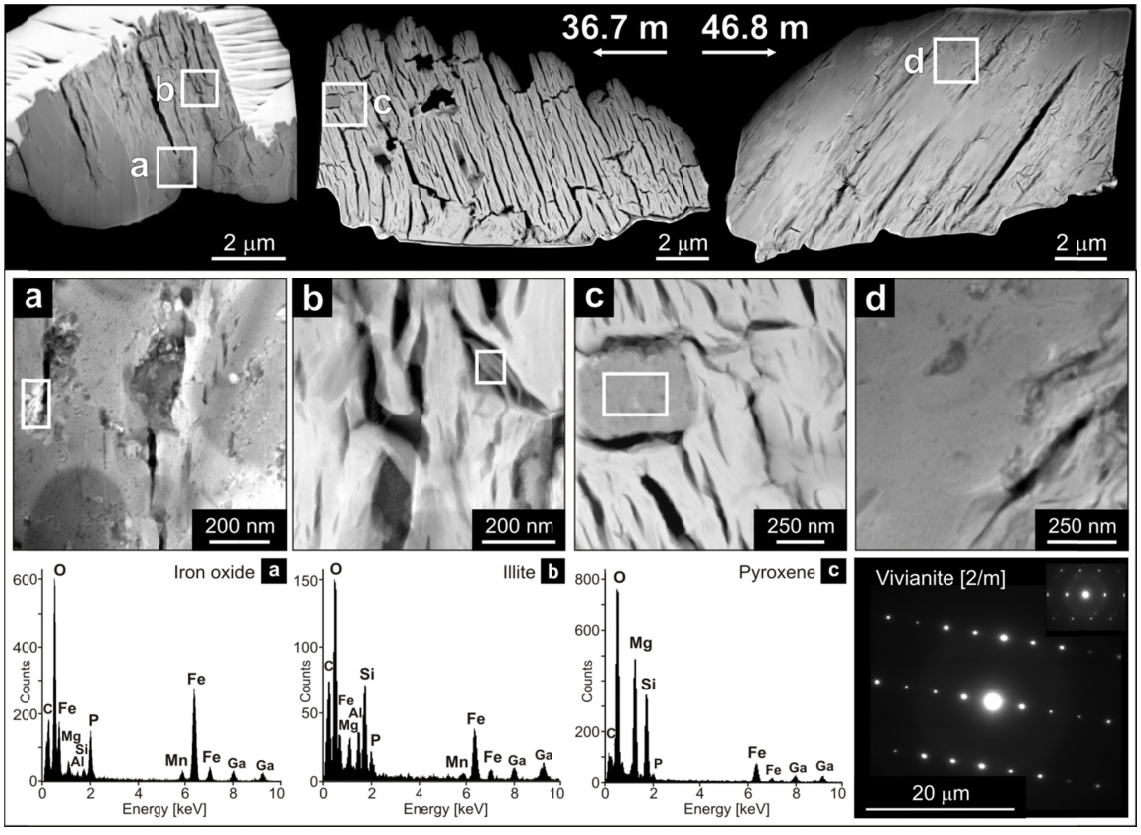

Figure 5: TEM images of vivianite crystal chunks, and close-ups to detrital inclusions with their EDX analyses and vivianite electron diffraction patterns. (Top) TEM images (distance: 330 mm) of vivianite crystal chunks from 36.7 and 46.8 m depth, showing that the crystal structure is denser in the deeper sample. **(Middle)** Close-ups of framed areas illustrate the presence of detrital inclusions within vivianite crystals, namely iron oxide (a), illite (b) and pyroxene (c). Image d demonstrates the denser structure of the vivianite crystal from 46.8 m depth. **(Bottom)** EDX spectra for iron oxide (a), illite (b) and pyroxene (c); and high-resolution electron diffraction pattern of the vivianites from 46.8 and 36.7 (insert) m depth providing evidence for an organized and less-organized monoclinic lattice.